

Preliminary study of feasibility of an experiment looking for excited state double beta transitions in Tin

Soumik Das^{1,2}, S. K. Ghorui^{2,*}, P. K. Raina², A. K. Singh¹, P. K. Rath³, F. Cappella⁴, R. Cerulli⁴, M. Laubenstein⁴, P. Belli⁵, R. Bernabei^{5,6}

¹*Dept. of Physics, Indian Institute of Technology Kharagpur, Kharagpur, IN-721302, India*

²*Dept. of Physics, Indian Institute of Technology Ropar, Ropar, IN-140001, India*

³*Dept. of Physics, University of Lucknow, Lucknow, IN-220628, India*

⁴*INFN, Laboratory Nazionali del Gran Sasso, I-67100 Assergi (AQ), Italy*

⁵*INFN sezione Roma "Tor Vergata", I-00133 Rome, Italy*

⁶*Dipartimento di Fisica, Università di Roma "Tor Vergata", I-00133 Rome, Italy*

Abstract

An attempt to study the feasibility of a new experiment to search for double beta decay in ^{112}Sn and ^{124}Sn was carried out by using ultra-low background HPGe detector (244 cm³) inside the Gran Sasso National Laboratory (LNGS) of the INFN (Italy). A small sample of natural Sn was examined for 2367.5 h. The radioactive contamination of the sample has been estimated. The data has also been considered to calculate the present sensitivity for the proposed search; half-life limits $\sim 10^{17} - 10^{18}$ years for $\beta^+\text{EC}$ and EC-EC processes in ^{112}Sn and $\sim 10^{18}$ years for $\beta^-\beta^-$ transition in ^{124}Sn were measured. In the last section of the paper the enhancement of the sensitivity for a proposed experiment with larger mass to reach theoretically estimated values of half-lives is discussed.

Keywords: Double beta decay, ultra low background, HPGe γ detector

1. Introduction

The existence of non-zero mass of neutrino has been established by neutrino flavor-oscillation experiments [1–3]. However, the nature of the neutrino, either Dirac or Majorana, can only be tested through observation of neutrino-less double beta decay, which is a rare second order transition involving two isobars. Moreover, the double beta decay experiments have the potential to establish the absolute scale of the neutrino mass, to prove the hierarchy of neutrino mass, to test the existence of right-handed admixtures in the weak interaction, and to test some other

*Corresponding author. *E-mail address:* surja@iitrpr.ac.in (S. K. Ghorui).

effects beyond the Standard Model. The $0(2)\nu\beta\beta$ decay can occur as :

$$(A, Z) \rightarrow (A, Z + 2) + 2e^- + (2\bar{\nu}_e) \quad (1)$$

$$(A, Z) \rightarrow (A, Z - 2) + 2e^+ + (2\nu_e) \quad (2)$$

$$e^- + (A, Z) \rightarrow (A, Z - 2) + e^+ + (2\nu_e) \quad (3)$$

$$2e^- + (A, Z) \rightarrow (A, Z - 2) + (2\nu_e) \quad (4)$$

Triggered by the important implication of neutrino mass, a new generation of experiments are aimed to observe $0\nu\beta\beta$ decay in various isotopes and with different experimental techniques [4]. Among the main experimental activities, we remind that recently three $\beta\beta$ experiments have published new experimental data: GERDA [5], EXO-200 [6] and KamLAND-Zen [7]. GERDA is searching for $0\nu\beta\beta$ decay in ^{76}Ge while EXO-200 and KamLAND-Zen are looking for the decay in ^{136}Xe . Several other experiments are going through their R&D phase. These include CUORE (^{130}Te) [8], SuperNEMO (^{82}Se) [9], MAJORANA (^{76}Ge) [10], SNO+ (^{130}Te) [11], NEXT (^{136}Xe) [12] etc.. Present experiments are sensitive to half-lives of the order of 10^{25} years and a corresponding effective mass of the neutrino $\langle m_{\beta\beta} \rangle \sim 100$ meV [13]. Constrained by the uncertainties in the calculation of nuclear transition matrix elements [14], phase space factor [15] and by the g_A value [16] that are used to determine $\langle m_{\beta\beta} \rangle$ as well as by the different background for different isotopes, it is essential to measure the half-life for $0\nu\beta\beta$ decay in several isotopes.

Although Sn was considered as one of the potential candidates since the 1980s [17], there have been only a few studies on Sn. It can be mentioned that one of the earliest attempts for the experimental study of double beta decay was done by Fireman [18] in 1949 using ^{124}Sn .

Natural tin contains three isotopes which can decay via double beta transition; $^{122,124}\text{Sn}$ through two electron mode and ^{112}Sn through $\beta^+\text{EC}$ and EC-EC processes, as given in the following:

$$^{122}\text{Sn} \rightarrow ^{122}\text{Te} + 2e^- + (2\bar{\nu}_e) \quad (5)$$

$$^{124}\text{Sn} \rightarrow ^{124}\text{Te} + 2e^- + (2\bar{\nu}_e) \quad (6)$$

$$e^- + ^{112}\text{Sn} \rightarrow ^{112}\text{Cd} + e^+ + (2\nu_e) \quad (7)$$

$$2e^- + ^{112}\text{Sn} \rightarrow ^{112}\text{Cd} + (2\nu_e) \quad (8)$$

The Q-values for the decay transitions in ^{112}Sn , ^{122}Sn and ^{124}Sn are 1919.82 ± 0.16 keV, 372.9 ± 2.7 keV and 2291.1 ± 1.5 keV [19], respectively. The natural isotopic abundances for these isotopes are 0.97(1)%, 4.63(3)% and 5.79(5)% [20], respectively. The gamma rays from ^{122}Sn decays are

at low energy where the background is high and makes it more difficult to study this decay modes in an external source experiment. Therefore, we have not considered this nucleus for the present study.

Recently, investigations were carried out using natural tin samples for $\beta^-\beta^-$ decay of ^{124}Sn to the excited states of the daughter nucleus ^{124}Te and $\beta^+\text{EC}$ and EC-EC processes in ^{112}Sn by Dawson *et al.* [21, 22], Kim *et al.* [23] and Barabash *et al.* [24]. Half-life limits of the order of $10^{18} - 10^{21}$ years were obtained in those experiments. Searches for $\beta^+\text{EC}$ and EC-EC processes in ^{112}Sn were also carried out by Kidd *et al.* [25] and Barabash *et al.* [26, 27] using enriched material obtaining the best half-life limit of 10^{21} years. The Kims collaboration [28] gave a half-life limit 2.0×10^{20} years for neutrino-less double beta decay of ^{124}Sn using tin-loaded liquid scintillator.

An attempt to study the feasibility of a new experiment to search for double beta decay in ^{112}Sn and ^{124}Sn was carried out using an ultra-low background HPGe detector. The gamma rays produced by the de-excitations of the excited levels of either ^{112}Cd or ^{124}Te can be detected by the HPGe detector. The aim of the present study was to investigate the decay processes to the ground state as well as to the excited states in ^{112}Sn and to the excited states in ^{124}Sn using γ -ray spectrometry. We will discuss in the last section also a possible enhancement of the sensitivity with a proposed experiment with larger mass to reach the half-life values estimated by theory.

2. Experimental set-up and measurements

A coaxial closed-end n-type ultra low background HPGe (GeBer) γ detector (244 cm^3) was used for the measurement. The detector is placed in the Gran Sasso National Laboratory (LNGS) of the INFN, Italy, located underground at ≈ 3600 meters of water equivalent. The schematic diagram of the experimental setup is shown in Fig. 1. The physical dimensions of the detector are given in Table 1. More details about the detector and the ultra low background setup can be found in [29].

Monte-Carlo simulation of HPGe detector has been performed using the GEANT4 software library [30]. To validate the results of the simulation, we have compared the simulated efficiencies with known experimental results. The full-energy-peak (FEP) efficiency of the HPGe detector was measured for different γ ray energies using ^{241}Am , ^{133}Ba , ^{137}Cs and ^{60}Co point sources. The sources were placed at a distance of 26.5 cm above the end cap of the detector. The energy resolution (FWHM) of the detector was measured as 2.0 keV at 1332.5 keV.

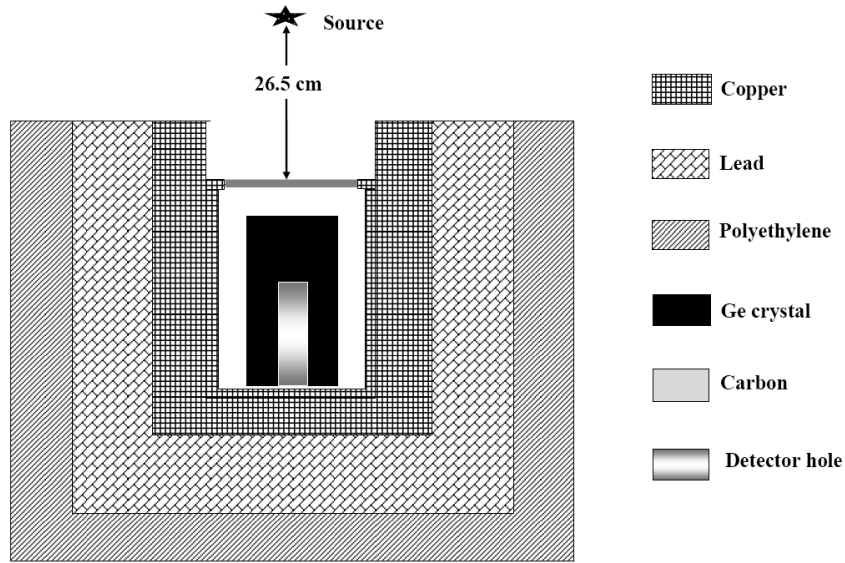


Figure 1: Schematic diagram of experimental set-up used in simulation. Figure not in scale.

A natural tin (purity 99.997%) sample of 13.3 g and with a thickness of 4.5 mm was placed on the end-cap, and the spectrum was measured with the HPGe detector in order to study the double beta decay processes in ^{112}Sn and ^{124}Sn nuclei. Data were accumulated for 2367.5 h with the sample and for 6109.4 h without the sample (background). The energy spectra of sample and background, normalized to the time of measurement of sample, are shown in Fig. 2.

3. Results and Discussion

3.1. Efficiency of the detector

The FEP efficiency of the detector was simulated for the calibrated point sources using Monte-Carlo based software libraries GEANT4 [30] and EGS4 [31]. Generally, the results of the Monte Carlo simulations deviate significantly ($> 10\%$) from the experimental results [32–38]. The difference can be due to two reasons: the uncertainties associated with the detector shape parameters provided by the manufacturer or incomplete charge collection in the crystal during the measurement process. Usually, all the information about the inner components of the germanium detector are not supplied by the manufacturer. Thus uncertainties arise due to

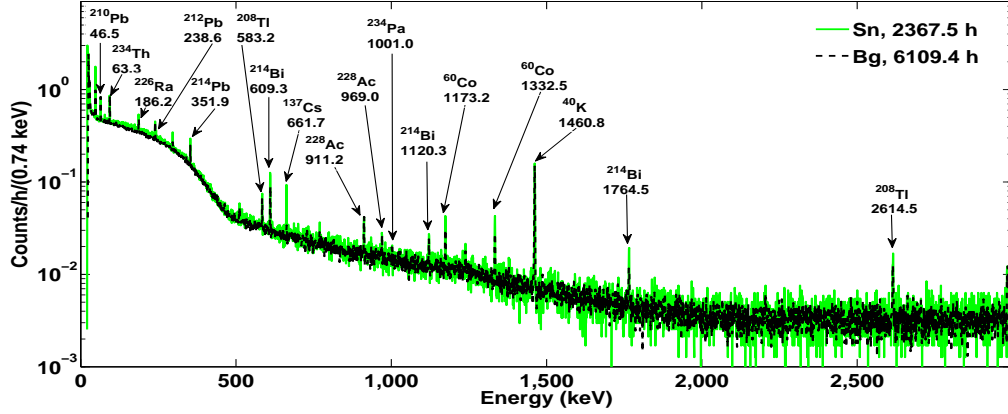


Figure 2: Energy spectrum with 13.3 g of natural tin sample (Sn) for 2367.5 h of measurement in comparison with background spectrum (Bg) of ultra low-background HPGe detector measured for 6109.4 h. The energy of the γ lines are in keV.

Table 1: The geometrical parameters of the detector. It is worth noting that the only difference between optimized and nominal values of the detector is the hole inner dead layer (0.3 mm nominal value). See text.

Detector parameter	Optimized value (MC2)(mm)
Ge crystal radius	30.85
Ge crystal length	81.70
Carbon (C) window thickness	0.76
Ge crystal-C window distance	4.00
Hole radius	4.95
Hole length	73.40
Ge side dead layer	0.0
Ge front dead layer	0.0
Hole inner dead layer	5.00

possible additional absorbers or on the nature of the materials allocated around the Ge crystal. Furthermore, the dimensions provided by the manufacturer correspond to the time of assembly of the detection system at room temperature. Then changes in the mechanical support of the crystal due to contractions at low temperature may lead to changes in the detector configurations [33]. There is also a certain uncertainty in the crystal parameters e.g. the dead layer thicknesses

Table 2: Comparison of experimental efficiency with simulated efficiency computed with two different Monte-Carlo codes: EGS4 (E4) and GEANT4 (G4). Efficiencies related to MC1 and MC2 are calculated considering two different thickness of the inner dead-layer: 1.5 mm and 5.0 mm, respectively.

Source	Energy	Exp	MC1	$\frac{Exp}{MC1}$	MC2	$\frac{Exp}{MC2}$	MC1	$\frac{Exp}{MC1}$	MC2	$\frac{Exp}{MC2}$
	keV	%	(E4)%	(E4)	(E4) %	(E4)	(G4)%	(G4)	(G4)%	(G4)
^{241}Am	26.3	0.0048	0.0064	75%	0.0064	75%	0.0066	73%	0.0064	75%
	59.5	0.0938	0.1089	86%	0.1088	86%	0.1135	83%	0.0974	96%
^{133}Ba	81.0+79.6	0.0913	0.1073	85%	0.1044	87%	0.1033	88%	0.0979	94%
	276.4	0.0111	0.0131	85%	0.0114	97%	0.0132	84%	0.0116	96%
	302.9	0.0270	0.0305	89%	0.0271	100%	0.0313	86%	0.0280	96%
	356.0	0.0798	0.0926	86%	0.0799	100%	0.0955	84%	0.0810	99%
	383.8	0.0110	0.0126	87%	0.0107	103%	0.0125	88%	0.0109	101%
^{137}Cs	661.7	0.0668	0.0818	82%	0.0679	98%	0.0948	71%	0.0690	97%
^{60}Co	1173.2	0.0527	0.0652	81%	0.0531	99%	0.0680	78%	0.0520	101%
	1332.5	0.0478	0.0600	80%	0.0476	100%	0.0636	75%	0.0480	100%

[34] or the distance between end cap and Ge crystal. It has also been observed, that there can be a substantial increase of the dead layer thickness after some years of operating time [35]. Therefore, to match the experimental efficiency values, the detector parameters and the dead layer thickness can be varied [38]. In the first step, the detector parameters provided by the manufacturer was used in the simulation. A fine adjustment was then made by varying only the inner dead layer thickness in a systematic way to match the experimental efficiency values. In order to show the dependence of the calculated efficiencies on the inner hole dead layer, the results obtained by considering two different thicknesses (1.5 mm and 5.0 mm) are compared with the experimental values in Table 2 and in Fig. 3. In the latter case the FEP efficiencies have been divided by the branching ratios of the corresponding γ rays. From Table 2, we can see that for the optimized dead layer of the inner hole, thickness of 5.0 mm, the simulated efficiencies (for both EGS4 and GEANT4) are in very good agreement with the experimental results except for the very low energy region. The uncertainty is within 4%, which is quite reasonable considering the statistical fluctuations. However, at very low energy, difference is quite large. This could be due to the very small mean free path of γ rays at this energy scale. Therefore, some γ rays are absorbed before reaching the detector. The optimized parameters were then used to calculate

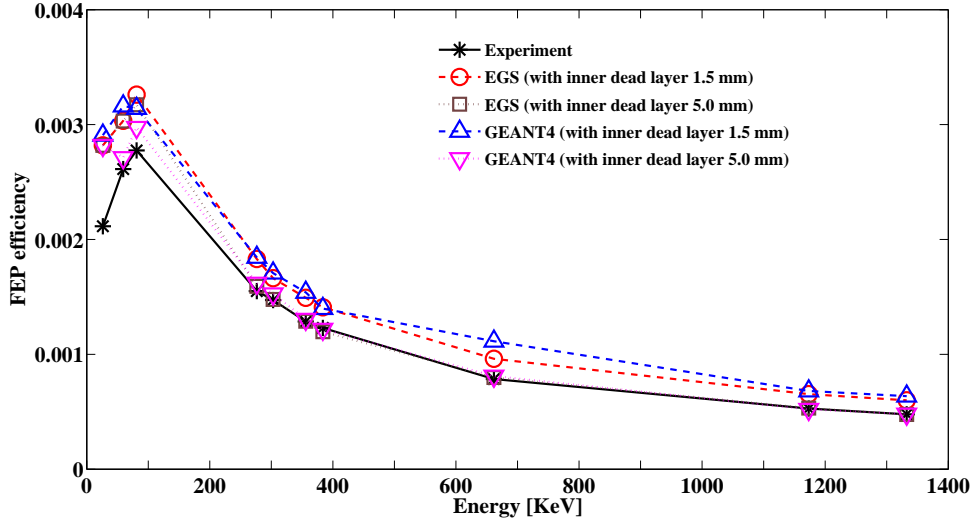


Figure 3: Comparison of the experimental efficiencies with those obtained from Monte-Carlo simulation using two different codes EGS4 and GEANT4. Here the FEP efficiencies have been divided by the branching ratios of the corresponding gammas.

the FEP efficiency for a volume source of dimensions equal to the tin sample used in the present work.

3.2. Radioactive contamination in the sample

The sources of background radiations measured in an underground laboratory can be classified into several categories; environmental radioactivity including radon, gamma rays, neutrons from natural fission and from the (α, n) reaction, radioactive impurities in the detector and shielding materials and cosmic rays with relevant contributions from muons and neutrons [39, 40]. In the measured spectra, background components can be identified by their characteristic γ -emission peaks. The specific activities of the radioactive nuclei present in the natural tin sample were calculated with the formula [29]

$$A = \frac{(S_s/t_s - S_b/t_b)}{m\eta}, \quad (9)$$

where S_s and S_b denote the area under a peak in the sample and background spectra, respectively. The measurement time of the sample and background spectra are denoted by t_s and t_b , respectively. The mass of the sample is represented by m and η is the efficiency of the full-energy peak detection (η also takes into account the decay fraction of the γ ray which was obtained

Table 3: The radioactive contamination present in the Tin sample measured with HPGe detector. Limits are given at 90 % C. L.

Source	Energy (keV)	Count rate (mBq) from Signal	Count rate (mBq) from background	η (%)	Activity in (mBq/Kg)
^{228}Ac	911.2	0.014±0.002	0.012±0.001	1.16	≤ 30
^{212}Pb	238.6	0.053±0.005	0.048±0.003	6.94	≤ 15
^{208}Tl	583.2	0.021±0.002	0.015±0.001	5.83	7±3
^{212}Bi	727.3	0.004±0.001	0.006±0.001	0.37	≤ 34
^{214}Bi	1764.5	0.098±0.001	0.006±0.001	0.41	42±22
^{214}Pb	351.9	0.048±0.004	0.033±0.002	3.81	30±9
^{210}Pb	46.5	0.335±0.008	0.196±0.004	1.30	801±51
^{234}Th	63.3	0.095±0.005	0.103±0.004	1.11	≤ 28
^{226}Ra	186.2	0.056±0.006	0.060±0.004	0.72	≤ 79
^{234m}Pa	1001.0	0.004±0.001	0.003±0.001	0.03	≤ 739
^{137}Cs	661.7	0.030±0.002	0.003±0.001	5.03	39±4
^{60}Co	1173.2	0.020±0.002	0.012±0.001	3.63	17±4
^{40}K	1460.8	0.094±0.003	0.087±0.002	0.34	155±79

from National Nuclear Data Center (NNDC) [41]). Activities of the natural radioactive sources present in the tin sample are listed in Table 3. Activity limits are given at 90 % confidence level (C. L.) according to the Feldman-Cousins method [42].

3.3. Double beta decay study of $^{112,124}\text{Sn}$

In the accumulated spectra with the tin sample, no peaks are observed which could be unambiguously attributed to the double beta decay processes of $^{112,124}\text{Sn}$. Therefore, only half-life limits are calculated using the formula

$$T_{1/2} \geq \frac{(\ln 2) \cdot N \cdot \eta \cdot t}{\text{lim } S}, \quad (10)$$

where N is the number of $\beta\beta$ -active nuclei, t is the measurement time and η is the FEP detection efficiency. The expression $\text{lim } S$ is the number of events of the effect searched for which can be excluded at a given C. L.. All the limits reported in the present study are given at 90% C. L.. The values of $\text{lim } S$ were calculated using the Feldman-Cousins procedure [42]. The detection

efficiencies of the double beta processes in the tin isotopes were calculated using the GEANT4 software library [30]. The DECAY0 [43] event generator has been used to generate the initial kinematics of the particles.

Taking into account the isotopic composition of natural tin, the sample contained 6.55×10^{20} nuclei of ^{112}Sn and 3.90×10^{21} nuclei of ^{124}Sn . The measured limits on half-lives for these two isotopes along with today's best experimental limits and theoretical estimates are reported in Table 4.

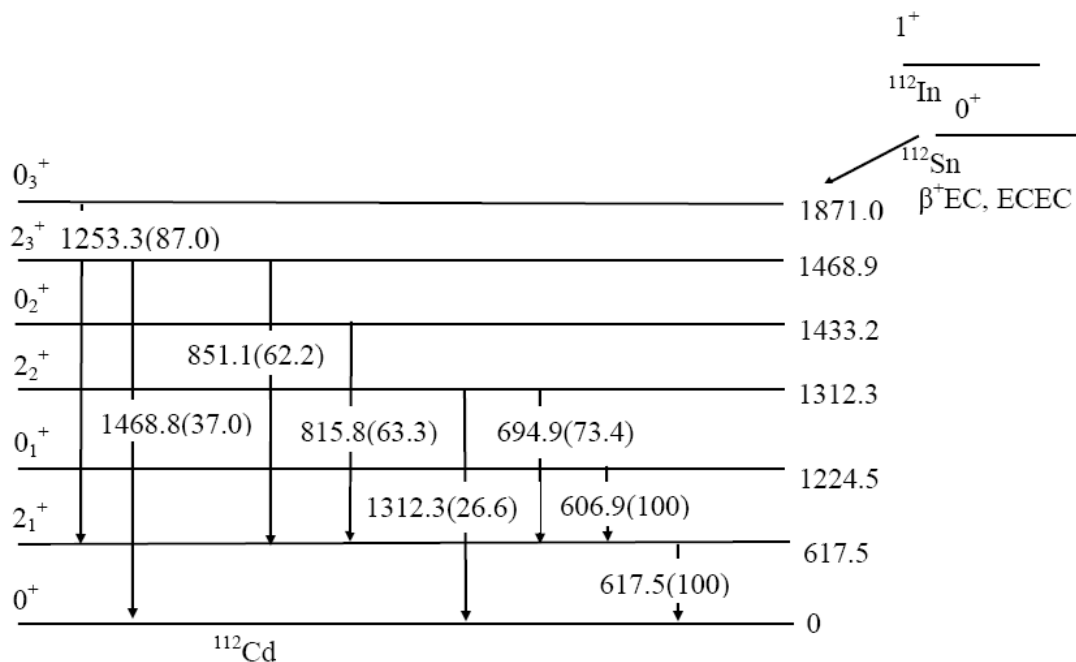


Figure 4: Partial decay scheme of ^{112}Sn [44]. The energies of the excited levels and the emitted γ quanta are in keV with relative intensities of γ quanta are given in parenthesis.

3.3.1. EC-EC decay of ^{112}Sn

In the 2ν EC-EC decay of ^{112}Sn to the ground state of ^{112}Cd , all the energy release is carried away by the neutrinos except for a very small amount emitted as X-rays. These X-rays lie below the energy threshold of the measurement apparatus. In case of the neutrino-less mode, bremsstrahlung γ quanta are emitted with an energy equal to $E_\gamma = Q_{2\beta} - \epsilon_1 - \epsilon_2 - E_{exe}$, where ϵ_i are electron binding energies of daughter nuclide, and E_{exe} is the populated level energy of ^{112}Cd . The partial decay scheme of ^{112}Sn is shown in Fig. 4 [44]. For the transition to the excited state, the bremsstrahlung γ quanta are accompanied by γ rays emitted from nuclear

de-excitation. We did not observe any peak with the expected energies for the EC-EC decay of ^{112}Sn . Only lower limits of half-lives are obtained using the Feldman-Cousins prescription [42]. The $T_{1/2}$ limits along with the γ energies and the corresponding detection efficiencies are shown in Table 4.

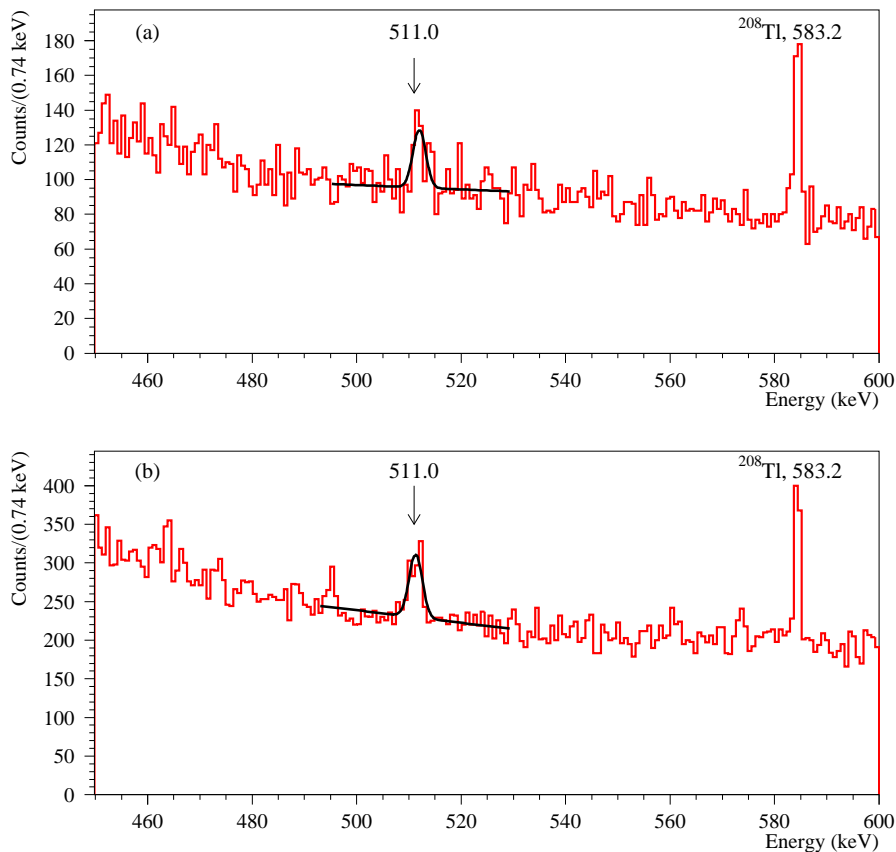


Figure 5: Part of the energy spectra accumulated with Sn sample for 2367.5 h of measurement by ultralow-background HPGe γ detector for energy range (450-600) keV (upper panel). The energy spectrum accumulated without the sample over 6109.4 h is also shown (lower panel). Fits of the 511 keV annihilation γ peaks are shown by solid line.

3.3.2. β^+EC processes in ^{112}Sn

The $(0\nu + 2\nu)\beta^+EC$ transition to the ground state of daughter nuclei is accompanied by two annihilation γ quanta with energy 511.0 keV. Moreover, the detector surroundings and the sample contains the radioactive element ^{208}Tl which emits γ quanta of energy 583.2 keV. The energy spectra accumulated with and without the sample in the energy interval 450-600 keV

are presented in Fig. 5. The measured area of the annihilation peak is (130 ± 7) counts. The area of the peak in the background spectrum is (100 ± 15) counts (normalized on the time of measurement with the tin sample). The excess of events in the data accumulated with the tin sample can be explained by radioactive contamination of the sample itself. In particular, the decay of ^{208}Tl contributes 17 ± 7 counts of 510.8 keV gamma quanta. The difference in the areas of the annihilation peak (13 ± 18) counts, which can be attributed to electron capture with positron emission in ^{112}Sn , gives no indication on the effect. In accordance with the Feldman-Cousins procedure, 42.6 counts can be excluded at 90% C.L. Taking into account the FEP efficiency (η) of 7.58%, the lower limit of the $(0\nu + 2\nu)\beta^+\text{EC}$ transition to the ground state is 2.18×10^{17} yr.

In the case of the $(0\nu + 2\nu)\beta^+\text{EC}$ transition to the excited 2_1^+ (617.5 keV) states of ^{112}Cd , no peak has been observed. The limit on the half-life is reported in Table 4. The theoretical $T_{1/2}$ is estimated to be very high because of the low phase space available for this transition.

3.3.3. The $\beta^-\beta^-$ decay of ^{124}Sn

For $\beta^-\beta^-$ decay of ^{124}Sn , only transitions to excited states of ^{124}Te can be studied as we are measuring gamma quanta. The partial decay scheme of ^{124}Sn is shown in Fig. 6 [45]. No peak has been observed at 602.7 keV, as shown in Fig. 7.

To derive the $\lim S$ value for the 602.7 keV γ -line, a model of the background was built from two Gaussian (one to describe the effect, and the second one to take into account the gamma peak with energy 609.3 keV of ^{214}Bi) plus first-degree polynomial to describe the continuous background. The best fit ($\chi^2/\text{n.d.f.} = 50.8/51 = 0.99$) achieved in the energy interval 586–628 keV gives the area of the peak searched for 2 ± 12 counts (at the energy 602.7 keV), which conservatively provides $\lim S = 22$ counts. Considering the transition to the 2_5^+ (2182.4 keV) state (studied here for the first time), the calculated efficiency to detect γ quanta with energy 602.7 keV is 4.06%, thus $T_{1/2} \geq 1.36 \times 10^{18}$ yr. The half-lives limits for the transition of ^{124}Sn to other excited states of ^{124}Te are reported in the lower part of Table 4.

The overall result is that due to the small mass of the tin sample (13.3 g), the obtained limits are rather poor compared to the existing experimental data. Therefore, it is certainly worthwhile to repeat the measurement with a larger sample, may be even enriched in the isotopes of interest, in order to obtain more stringent limits.

Table 4: The experimental limits and theoretical predictions for β^+ EC/ECEC decay in ^{112}Sn and $\beta^-\beta^-$ decay in ^{124}Sn .

Transition	Mode	Energy of γ rays (keV)	η (%)	$LimS$ 90% C. L	$T_{1/2}^{exp}$ (yr) at 90% C. L.		$T_{1/2}^{th}(2\nu)$ (yr) [46, 47]
					Present work	Previous work [24, 27]	
$^{112}\text{Sn} \rightarrow ^{112}\text{Cd}$							
β^+ EC; g.s.	$0\nu + 2\nu$	511.0	7.58	42.6	2.18×10^{17}	0.92×10^{20}	3.8×10^{24}
β^+ EC; 2_1^+ 617.5	$0\nu + 2\nu$	617.5	5.95	7.8	9.40×10^{17}	7.02×10^{20}	2.3×10^{32}
ECEC; K^1L^2 ;g.s.	0ν	1889.1	2.16	2.1	12.68×10^{17}	8.15×10^{20}	–
ECEC; 2_1^+ 617.5	0ν	617.5	4.59	7.8	7.25×10^{17}	9.40×10^{20}	–
ECEC; 0_1^+ 1224.4	0ν	606.9	3.32	40.2	1.02×10^{17}	12.86×10^{20}	–
		617.5	3.22	7.8	5.09×10^{17}	–	–
ECEC; 2_2^+ 1312.3	0ν	617.5	2.35	7.8	3.71×10^{17}	8.89×10^{20}	–
		694.7	2.11	35.9	0.72×10^{17}	–	–
		1312.3	0.86	18.0	0.59×10^{17}	–	–
ECEC; 0_2^+ 1433.2	0ν	617.5	2.85	7.8	4.50×10^{17}	6.86×10^{20}	–
		815.8	1.01	32.0	0.39×10^{17}	–	–
ECEC; 2_3^+ 1468.8	0ν	617.5	2.06	7.8	3.26×10^{17}	6.46×10^{20}	–
		851.1	1.59	6.0	3.27×10^{17}	–	–
		1468.8	1.05	5.2	2.49×10^{17}	–	–
ECEC; 0_3^+ 1871.14	0ν	617.5	4.76	7.8	7.52×10^{17}	13.43×10^{20}	–
		1253.4	2.72	24.4	1.37×10^{17}	–	–
ECEC; 2_1^+ 617.5	2ν	617.5	6.06	7.8	9.58×10^{17}	11.94×10^{20}	4.9×10^{28}
ECEC; 0_1^+ 1224.4	2ν	606.9	4.26	40.2	1.30×10^{17}	16.25×10^{20}	7.4×10^{24}
		617.5	4.51	7.8	7.13×10^{17}	–	–
ECEC; 2_2^+ 1312.3	2ν	617.5	3.26	7.8	5.15×10^{17}	11.24×10^{20}	1.9×10^{32}
		694.7	2.96	35.9	1.01×10^{17}	–	–
		1312.3	1.25	18.0	0.85×10^{17}	–	–
ECEC; 0_2^+ 1433.2	2ν	617.5	3.90	7.8	6.16×10^{17}	8.64×10^{20}	–
		815.8	1.39	32.0	0.54×10^{17}	–	–
ECEC; 2_3^+ 1468.8	2ν	617.5	2.80	7.8	4.42×10^{17}	8.19×10^{20}	6.2×10^{31}
		851.1	2.15	6.0	4.42×10^{17}	–	–
		1468.8	1.42	5.2	3.37×10^{17}	–	–
ECEC; 0_3^+ 1871.14	2ν	617.5	4.76	7.8	7.52×10^{17}	13.43×10^{20}	5.4×10^{34}
		1253.4	2.72	24.4	1.37×10^{17}	–	–
$^{124}\text{Sn} \rightarrow ^{124}\text{Te}$							
$\beta^-\beta^-$; 2_1^+ 602.7	$0\nu+2\nu+0\nu\chi^0$	602.7	6.05	22.0	2.02×10^{18}	9.1×10^{20}	4.8×10^{23}
$\beta^-\beta^-$; 2_2^+ 1325.5	$0\nu+2\nu+0\nu\chi^0$	602.7	3.94	22.0	1.32×10^{18}	9.4×10^{20}	2.5×10^{27}
		722.8	3.40	28.0	0.89×10^{18}	–	–
$\beta^-\beta^-$; 0_1^+ 1657.3	$0\nu+2\nu+0\nu\chi^0$	602.7	4.59	22.0	1.54×10^{18}	12.0×10^{20}	–
		1054.5	3.21	2.7	8.71×10^{18}	–	–
$\beta^-\beta^-$; 0_2^+ 1882.9	$0\nu+2\nu+0\nu\chi^0$	557.4	3.70	7.6	3.57×10^{18}	12.0×10^{20}	–
		602.7	2.86	22.0	0.96×10^{18}	–	–
		722.8	2.51	28.0	0.66×10^{18}	–	–
$\beta^-\beta^-$; 2_3^+ 2039.4	$0\nu+2\nu+0\nu\chi^0$	602.7	3.07	22.0	1.03×10^{18}	8.6×10^{20}	–
		1436.7	1.57	2.3	5.00×10^{18}	–	–
$\beta^-\beta^-$; 2_4^+ 2091.6	$0\nu+2\nu+0\nu\chi^0$	602.7	4.60	22.0	1.54×10^{18}	9.6×10^{20}	–
		1488.9	2.31	2.8	6.04×10^{18}	–	–
$\beta^-\beta^-$; 0_3^+ 2153.3	$0\nu+2\nu+0\nu\chi^0$	602.7	3.19	22.0	1.07×10^{18}	9.5×10^{20}	–
		722.8	2.04	28.0	0.54×10^{18}	–	–
		827.8	2.26	26.4	0.63×10^{18}	–	–
		1550.4	0.56	5.8	0.71×10^{18}	–	–
$\beta^-\beta^-$; 2_5^+ 2182.4	$0\nu+2\nu+0\nu\chi^0$	602.7	4.06	22.0	1.36×10^{18}	–	–
		1579.7	1.86	5.3	2.57×10^{18}	–	–

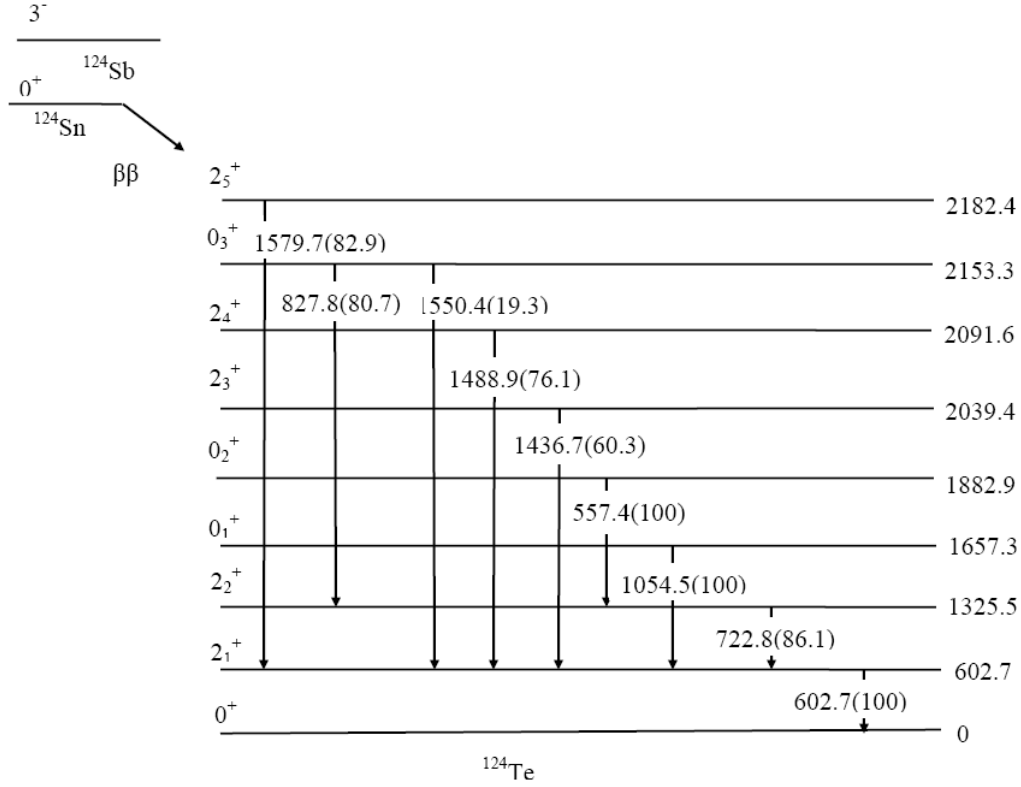


Figure 6: Partial decay scheme of ^{124}Sn [45]. The energies of the excited levels and of the γ quanta are in keV with relative intensities of γ quanta are given in parenthesis.

4. Double beta decay study with enhanced sensitivity

The sensitivity of a future experiment can be enhanced by either increasing the mass of the sample and the efficiency of the detector or by reducing the background. The efficiency of the detector depends on the position and the shape of the sample. The γ rays can undergo either self-attenuation to loose in the sample itself or absorption in other interposed media. The intensity of the gamma ray decreases to half of its initial value passing through a thickness of a half-value layer (HVL). The HVL depends on the atomic number of the element and also on the energy of the γ ray. HVL for tin material at different γ -ray energies were calculated from the mass attenuation coefficients (μ/ρ) values at different energies taken from NIST data [48].

Efficiencies of the detector were simulated for various sample thicknesses and different sample-detector distances. At a fixed γ ray energy, though the efficiency initially increases for lower energy upto 400 keV and then decreases with an increasing thickness of the sample as shown

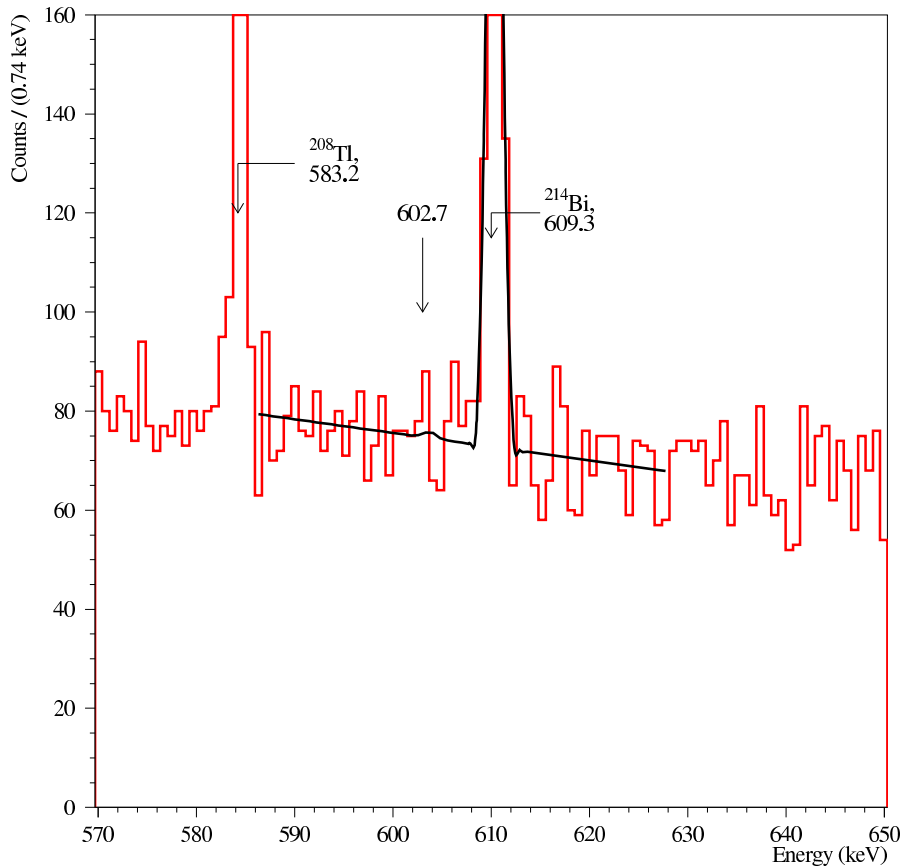


Figure 7: Part of the energy spectra accumulated with Sn sample for 2367.5 h of measurement. In particular, the region around the 602.7 keV peak, expected for the $\beta^-\beta^-$ processes in ^{124}Sn to the excited states of ^{124}Te , is shown. Fits of the excluded peak at energy 602.7 keV along with peak due to ^{214}Bi with energy 609.3 keV are depicted. Peak of ^{208}Tl with energy 583.2 keV is also shown.

in Fig. 8, the number of double beta nuclei increases with increasing the mass of the sample. Hence, the product of the efficiency and the number of nuclei together increases with increase in the mass of the sample as shown in Fig. 9.

For a cylindrical sample of fixed radius, the growth of the FEP count tends to saturate at a certain sample thickness as shown in Fig. 9. With further increase in sample thickness, the FEP count alters very less but the Compton continuum due to high energy photons increases. As a result of the increased Compton background, the important low-intensity gamma-lines emitted due to double-beta decay processes may not be detected experimentally. Therefore, it is very important to optimized the sample thickness. The optimization of sample thickness for cylindrical

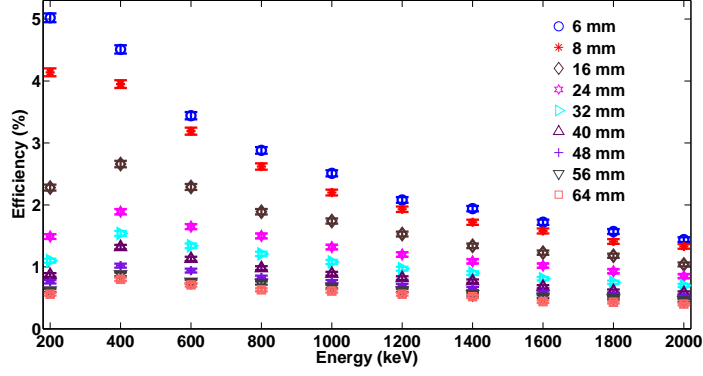


Figure 8: Detection efficiency of the HPGe detector at different energies in the region-of-interest for different thicknesses of the sample are shown. Legends are the thicknesses of the sample.

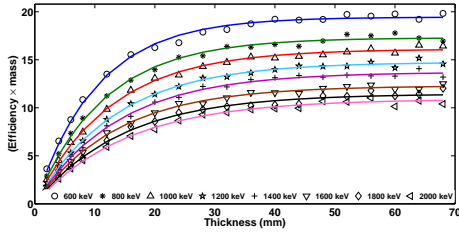


Figure 9: Comparison of efficiency times mass of the sample for different thicknesses of the sample.

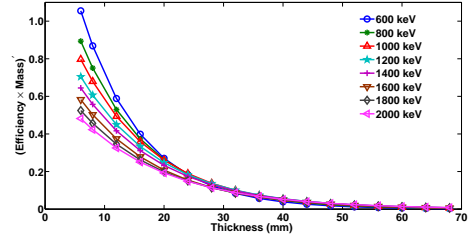


Figure 10: Correlation between sample thickness and first derivative of efficiency times mass of the sample.

geometry that maximizes the detection efficiency are studied by Barrera et al. [49], Shweikani et al. [50] and Li et al. [51] for HPGe detectors. For a cylindrical sample volume with fixed radius, optimal thickness has been determined by calculating the minimum value of the thickness that makes the first derivative of the sample mass multiplied by the detection efficiency nearly zero [50]. The correlation between sample thickness and efficiency times mass of the sample can be expressed by the Box Lucas function having the form [50] :

$$\eta \cdot M = a(1 - e^{-b \cdot h}) \quad (11)$$

where a , b are two constants and h is sample thickness. The variation of $(\eta \cdot M)$ with sample thickness is shown in Fig. 9. In order to estimate the optimum sample thickness at a given energy, the correlation between the first derivative of efficiency times mass of the sample, $(\eta \cdot M)'$ and sample thickness was studied. From Fig. 10, we can see that the value of $(\eta \cdot M)'$ tends nearly to zero at sample thickness 36 mm and higher for gamma energies 600-2000 keV. We consider

$h = 36$ mm as optimal thickness for the future large-scale experiment.

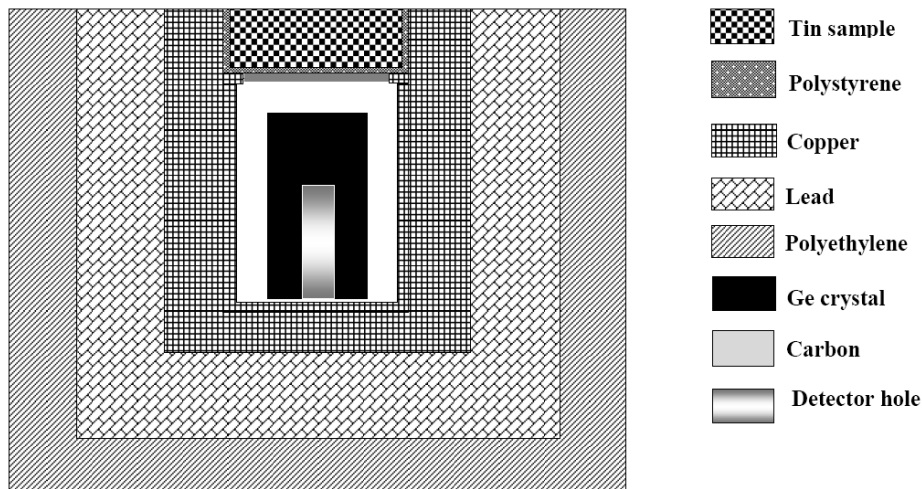


Figure 11: Schematic diagram of the experimental set-up of the proposed future experiment. Figure is not in scale.

Considering the geometry of the present HPGe detector, a cylindrical shaped ($\varnothing 86.0$ mm \times 36.0 mm) tin sample of mass ~ 1530 g (density of tin is taken as 7.31 g/cm³) can be placed on the sample holder, as shown in Fig. 11. A tin sample, enriched in ^{112}Sn up-to 90%, will contain 7.40×10^{24} nuclei of this isotope. Enriching in ^{124}Sn instead by the same factor, the sample will contain 6.68×10^{24} nuclei of it. Considering the efficiencies 2.44 % (2ν EC-EC) and 2.36 % (0ν EC-EC) for decay of ^{112}Sn to the 2_1^+ (617.5 keV) state of ^{112}Cd , the following sensitivity limits (at 90% C. L.) could be reached after two years of measurements:

$$T_{1/2}^{2\nu EC-EC} (^{112}\text{Sn, g.s.} \rightarrow 617.5 \text{ keV}) \geq 3.0 \times 10^{22} \text{ yr},$$

$$T_{1/2}^{0\nu EC-EC} (^{112}\text{Sn, g.s.} \rightarrow 617.5 \text{ keV}) \geq 3.0 \times 10^{22} \text{ yr}.$$

This result would be better than the previously measured best half-life limit[27]. For the double-beta decay transition of ^{124}Sn to the excited 2_1^+ (602.7 keV) state of ^{124}Te , with 90% enriched ^{124}Sn and an efficiency of 2.50 %, the sensitivity would be the same as for ^{112}Sn , up to 10^{22} yr (at 90% C. L.) for the half-life.

5. Conclusion

In our preliminary study for the search of excited state transitions concerning possible double beta decays of tin isotopes with a HPGe detector, we measured half-life limits of $10^{17} - 10^{18}$ yr for β^+ EC and EC-EC processes in ^{112}Sn and 10^{18} yr for $\beta^-\beta^-$ transition in ^{124}Sn . For the $0\nu\text{EC-EC}$ decay of ^{112}Sn to the ground state of its daughter nuclide we obtained a half-life limit of 1.27×10^{18} yr. We showed that an experiment with larger mass, and material enriched to high levels of either ^{112}Sn or ^{124}Sn , could reach with the same HPGe detector half-life limits for both tin isotopes on the order of 10^{22} yr for the decays to the excited levels. In India, an effort has been started to build up a bolometric Sn detector for experimental study of $0\nu\beta\beta$ decay in ^{124}Sn [52]. The experimental setup will be housed at upcoming India-based Neutrino Observatory site.

6. Acknowledgement

The authors would like to thank Prof. V. I. Tretyak, Prof. V. Nanal and Prof. R. G. Pillay for fruitful discussions and Gran Sasso laboratory staff for their technical assistance in running the experiment. Author Soumik Das would like to acknowledge the financial assistance from University Grant Commission, India (F No 10-2(5)/2006(ii)-EUII) and P. K. Raina, S. K. Ghorui and P. K. Rath acknowledge the financial support of the Council for Scientific and Industrial Research, India (CSIR Project No 03(1216)/12/EMR II) and Department of Science and Technology (DST), India (SB/S2/HEP-007/2013) for financial assistance during this work. Financial supports from DST, India (sanction order no. INT/Italy/p-7/2012(ER)) and MAE, Italy (Project Id : IN12MO11) are also acknowledged. We acknowledge the use of the computing facility from DST-FIST (Phase-II) Project installed in the Department of Physics, IIT Kharagpur, India.

References

- [1] Y. Fukuda, et al., Physical Review Letters 81 (1998) 1562.
- [2] Q. R. Ahmed, et al., Physical Review Letters 89 (2002) 011301.
- [3] K. Eguchi, et al., Physical Review Letters 90 (2003) 021802.
- [4] A. S. Barabash, Journal of Physics G: Nuclear and Particle Physics 39 (2012) 085103.

- [5] K. -H. Ackermann, et al., *European Physical Journal C* 73 (2013) 2330; M. Agostini, et al., *Physical Review Letters* 111 (2013) 122503.
- [6] J. B. Albert et. al., [The EXO-200 Collaboration], *Nature* 510 (2014) 229.
- [7] A. Gando, et al., *Physical Review Letters* 110 (2013) 062502.
- [8] C. Arnaboldi, et al., *Nuclear Instruments and Methods in Physics Research A* 518 (2004) 775.
- [9] R. Arnold, et al., *European Physical Journal C* 70 (2010) 927.
- [10] N. Abgrall, et al., *Advances in High Energy Physics* 2014 (2014) 365432.
- [11] A. Maio, [SNO+ Collaboration], *Journal of Physics: Conference Series* 587 (2015) 012030; S. Biller, arXiv:1405.3401v1 [physics.ins-det]
- [12] J. J. Gómez Cadenas et. al. [The NEXT Collaboration], *Advances in High Energy Physics* 2014 (2014) 907067.
- [13] O. Cremonesi, M. Pavan, *Advances in High Energy Physics* 2014 (2014) 951432.
- [14] P. K. Rath, et al., *Physical Review C* 88 (2013) 064322.
- [15] J. Kotila, F. Iachello, *Physical Review C* 85 (2012) 034316; S. Stoica, M. Mirea, *Physical Review C* 88 (2013) 037303.
- [16] S. Dell’Oro, S. Marcocci, and F. Vissani, *Physical Review D* 90 (2014) 033005.
- [17] M. Doi, T. Kotani, E. Takasugi, *Progress of Theoretical Physics Supplements* 83 (1985) 1.
- [18] E. L. Fireman, *Physical Review* 75 (1949) 323.
- [19] M. Wang, et al., *Chinese Physics C* 36 (2012) 1603.
- [20] M. Berglund, M. Wieser, *Pure and Applied Chemistry* 83 (2011) 397.
- [21] J. Dawson, et al., *Nuclear Physics A* 799 (2008) 167.
- [22] J. Dawson, et al., *Physical Review C* 78 (2008) 035503.
- [23] H. J. Kim, et al., *Nuclear Physics A* 793 (2007) 171.
- [24] A. S. Barabash, et al., *Nuclear Physics A* 807 (2008) 269.

- [25] M. F. Kidd, J. H. Esterline, W. Tornow, *Physical Review C* 78 (2008) 035504.
- [26] A. S. Barabash, et al., *Physical Review C* 80 (2009) 035501.
- [27] A. S. Barabash, et al., *Physical Review C* 83 (2011) 045503.
- [28] M. J. Hwang, et al., *Astroparticle Physics* 31 (2009) 412.
- [29] P. Belli et al., *Nuclear Physics A* 824 (2009) 101.
- [30] S. Agostinelli, et al., *Nuclear Instruments and Methods in Physics Research Section A* 506 (2003) 250; <http://geant4.web.cern.ch/geant4>, 2014.
- [31] W. R. Nelson et al., SLAC-Report-265, Stanford (1985) (unpublished).
- [32] <http://www.lns.sci.osaka-u.ac.jp/lab/annual/2003/Page-055.pdf>;
http://shodhganga.inflibnet.ac.in/bitstream/10603/4710/14/14_chapter%205.pdf
- [33] P. N. Johnston, P. A. Burns, *Nuclear Instruments and Methods in Physics Research Section A* 353 (1994) 101.
- [34] E. Chham et al., *Applied Radiation and Isotopes* 95 (2015) 30.
- [35] N. Q. Huy, D. Q. Binh, V. X. An, *Nuclear Instruments and Methods in Physics Research Section A* 573 (2007) 384.
- [36] T. Azli, Z. Chaoui, *Applied Radiation and Isotopes* 97 (2015) 106.
- [37] F. P. Cabal et al., *Applied Radiation and Isotopes* 68 (2010) 2403.
- [38] S. Hurtado, M. Garcia-Leon, R. Garcia-Tenorio, *Nuclear Instruments and Methods in Physics Research Section A* 518 (2004) 764.
- [39] M. Haffke, et al., *Nuclear Instruments and Methods in Physics Research Section A* 643 (2011) 36.
- [40] C. Dörr, H. V. Klapdor-Kleingrothaus, *Nuclear Instruments and Methods in Physics Research Section A* 513 (2003) 596.
- [41] [NNDC Database] <http://www.nndc.bnl.gov>, 2014.
- [42] G. F. Feldman, R. D. Cousins, *Physical Review D* 57 (1998) 3873.

- [43] O. A. Ponkratenko, V. I. Tretyak, Yu. G. Zdesenko, *Physics of Atomic Nuclei* 63 (2000) 1355.
- [44] D. de Frenne, E. Jacobs, *Nuclear Data Sheets* 79 (1996) 639.
- [45] J. Katakura, Z. D. Wu, *Nuclear Data Sheets* 109 (2008) 1655.
- [46] P. Domin, et al., *Nuclear Physics A* 753 (2005) 337.
- [47] J. Suhonen, *Nuclear Physics A* 864 (2011) 63.
- [48] C. T. Chantler, *Journal of Physical and Chemical Reference Data* 24 (1995) 71.
- [49] M. Barrera, et al., *Nuclear Instruments and Methods in Physics Research Section A* 421 (1999) 163.
- [50] R. Shweikani, et al., *Radiation Measurements* 70 (2014) 34.
- [51] Gang Li, et al., *Journal of Instrumentation* 10 (2015) P03010.
- [52] V. Nanal, INPC 2013 proceedings, *EPJ Web of Conferences* 66 (2014) 08005.